Biochimica et Biophysica Acta 1833 (2013) 559–572

Contents lists available at SciVerse ScienceDirect

Biochimica et Biophysica Acta

journal homepage: www.elsevier.com/locate/bbamcr

Ubiquitin C-terminal Hydrolase 37, a novel predictor for hepatocellular carcinoma recurrence, promotes cell migration and invasion via interacting and deubiquitinating PRP19

Ying Fang [a], Da Fu [a], Wenqing Tang [a], Yu Cai [a], Duan Ma [b], Huijun Wang [b], Ruyi Xue [a], Taotao Liu [a], Xiaowu Huang [c], Ling Dong [a], Hao Wu [a], Xizhong Shen [a,*]

[a] The Department of Gastroenterology of Zhongshan Hospital, Fudan University, Shanghai, 200032, PR China
[b] Key Laboratory of Molecular Medicine, Ministry of Education, Department of Biochemistry and Molecular Biology, Institutes of Medical Sciences, Shanghai Medical College, Fudan University, Shanghai, 200032, PR China
[c] Liver Cancer Institute of Zhongshan Hospital, Fudan University, Shanghai, 200032, PR China

ARTICLE INFO

Article history:
Received 1 August 2012
Received in revised form 11 November 2012
Accepted 25 November 2012
Available online 4 December 2012

Keywords:
UCH37
PRP19
Migration
Invasion
HCC

ABSTRACT

Ubiquitin C-terminal hydrolase 37 (UCH37) plays a crucial role in numerous biological processes and is also involved in oncogenesis. In this study, clinicopathologic data showed that UCH37 was over-expressed in hepatocellular carcinoma (HCC) cancerous tissues and was a significant predictor for time to recurrence (TTR). In vitro, we discovered that UCH37 could promote cell migration and invasion. Subsequently, we utilized Isobaric Tags for Relative and Absolute Quantitation (iTRAQ) to identify differentially expressed proteins in UCH37 over-expressing cells compared with the control cells, and found that PRP19, an essential RNA splicing factor, was up-regulated. The relationship between UCH37, PRP19 and the capability of cell migration and invasion was further confirmed. Collectively, this study demonstrated that UCH37 could promote cell migration and invasion in HCC cell lines through interacting and deubiquitinating PRP19, and suggested that UCH37 could be a novel predictor for HCC recurrence after curative resection.

1. Introduction

Hepatocellular carcinoma (HCC) is the fifth most common cancer and the third most common cause of cancer-related mortality in the world [1]. Its incidence and mortality rates have increased in recent years [2], and the high rate of recurrence or metastasis after curative resection remains one major obstacle for further improving the prognosis of HCC patients [3,4]. Several prognostic biomarkers in HCC have been reported recently [5–7]. Among these, alpha-fetoprotein (AFP) is still the best marker to supervise the recurrence and metastasis in AFP-positive HCC patients after operation [8]. Nevertheless, it is still difficult to predict prognosis in early-stage HCC in the AFP-normal patients [3,9]. Therefore, it is important to determine molecular signatures that define the risk of recurrence and metastatic potential of HCC. And such markers would allow appropriate therapeutic regimens to be applied earlier in the disease course.

Ubiquitin (Ub), a 76-amino-acid polypeptide, is ubiquitously distributed and highly conserved throughout eukaryotic organisms. Over the last few decades, conjugation of Ub and ubiquitin-like proteins to intracellular proteins has emerged as a critical regulatory process in virtually all aspects of cell biology [10–12]. Nevertheless, it is well recognized that protein ubiquitination, like protein phosphorylation, is a highly reversible process that can be regulated in the cell. Deubiquitinating enzymes (DUBs), capable of removing Ub from protein substrates, are also involved in numerous biological processes such as transcriptional regulation, growth and differentiation, and oncogenesis [13–15]. The ubiquitin C-terminal hydrolase (UCH), a subfamily of DUBs, prefers to cleave relatively small protein substrates

Abbreviations: 2D, two-dimensional; ABC, avidin–biotin complex; ACN, acetonitrile; AFP, alpha-fetoprotein; BAP1, BRCA1-associated protein-1; BCLC, Barcelona Clinic Liver Cancer; co-IP, co-immunoprecipitation; CT, computed tomography; DAB, diaminobenzidine; DDR, DNA damage response; DTT, dithiothreitol; DUBs, deubiquitinating enzymes; ESCC, esophageal squamous cell carcinoma; FA, formic acid; FBS, fetal bovine serum; FITC, fluorescein isothiocyanate; GO, Gene Ontology; HCC, hepatocellular carcinoma; HCD, higher-energy collision dissociation; hINO80, human Ino80 chromatin-remodeling complex; IAM, iodoacetamide; ICLs, interstrand cross-links; iTRAQ, Isobaric Tag for Relative and Absolute Quantitation; KEGG, Kyoto Encyclopedia of Genes and Genomes; MRI, magnetic resonance imaging; MS, mass spectroscopy; NTC, NineTeen associated-Complex; OS, Overall survival; PBS, phosphate-buffered saline; pI, isoelectric point; PI, propidium iodide; SCX, strong cation exchange; SD, standard deviation; shRNA, small hairpin RNA; siRNA, small interfering RNA; TEAB, triethylammonium bicarbonate; TNM, tumor-node-metastasis; TTR, time to recurrence; Ub, ubiquitin; UCH, ubiquitin C-terminal hydrolase; UPP, ubiquitin proteasome pathway; US, ultrasonography; WB, western blotting

* Corresponding author at: Department of Gastroenterology of Zhongshan Hospital, Fudan University, 180 Fenglin Rd, Shanghai 200032, PR China. Tel.: +86 21 64041990; fax: +86 21 64038038.
E-mail address: shen.xizhong@zs-hospital.sh.cn (X. Shen).

0167-4889/$ – see front matter © 2012 Elsevier B.V. All rights reserved.
http://dx.doi.org/10.1016/j.bbamcr.2012.11.020

from the C-terminus of Ub [16]. In UCH family, there are four known members: UCH-L1, UCH-L3, UCH37, and BRCA1-associated protein-1 (BAP1).

In our preliminary study, total proteins extracted from one human HCC tissue and one normal liver tissue were separated by two-dimensional (2D) gel electrophoresis, followed by silver staining. Among all protein spots analyzed, about 200 protein spots were found to be significantly altered between the cancerous tissue and the normal tissue. With molecular masses ranging from 25 to 40 kDa and isoelectric point (pI) between 5 and 6, nine protein spots were found in the cancerous tissue, but not in the normal tissue (Supplementary Fig. 1A). We presumed that UCH37 (molecular mass: 37 kDa; pI: 5.23) was one of the differentially expressed proteins. Subsequently, UCH37 mRNA expression was detected by real-time PCR in 22 HCC cases to confirm the hypothesis. Consequently, we found that UCH37 mRNA expression in the cancerous tissue was significantly higher than that in the non-cancerous tissue (Supplementary Fig. 1B). Meanwhile, we chose one of the HCC tissues and one of the normal liver tissues for western blotting and found that UCH37 was highly expressed in the cancerous tissue, but weakly expressed in the adjacent non-cancerous liver and normal liver tissue (Supplementary Fig. 1C). These were inspiring findings and indicated that there was likely relationship between UCH37 and HCC.

UCH37 is a protein of 329 amino acids, which is well conserved from fungi to humans [17]. Previous studies have focused on the deubiquitination mechanism of UCH37. It is responsible for the Ub isopeptidase activity in the 19S proteasome regulatory complex, which is different from other UCH members, showing that neither UCH37 alone nor the UCH37–Adrm1 or UCH37–Adrm1–hRpn2 complexes can hydrolyze Lys48-linked di-ubiquitin efficiently; that rather, their incorporation into the 19S complex is required to enable UCH37 to process large ubiquitin protein conjugates such as di-ubiquitin [17–19]. Further studies have suggested that UCH37 is associated with the human Ino80 chromatin-remodeling complex (hINO80) in the nucleus and can be activated via transient association of 19S regulatory particle- or proteasome-bound hRpn13 with hINO80 [20,21]. Although there is growing evidence that UCH enzymes and human malignancies are closely correlated [22], the biological roles of UCH37 have not been determined.

In the current study, we found out that UCH37 was highly expressed in HCC cancerous tissues and explored the predictive value of UCH37 for HCC recurrence after curative resection. Furthermore, we discovered that UCH37 could promote cell migration and invasion in HCC cell lines through interacting and deubiquitinating PRP19, an essential RNA splicing factor.

2. Material and methods

2.1. Patients and follow-up

Tumor specimens used in the current study were obtained from 90 HCC patients who underwent curative resection at Liver Cancer Institute, Zhongshan Hospital, Fudan University from October 1, 2006 to December 31, 2008. The inclusion and exclusion criteria of the patients included (1) having a distinctive pathologic diagnosis of HCC; (2) having no anti-cancer treatment before liver resection; (3) having curative liver resection; (4) having suitable formalin-fixed, paraffin-embedded tissues; and (5) having a complete clinicopathologic and follow-up data.

Curative resection was defined as: (1) complete resection of all tumor nodules and the surgical free margin of more than 5 mm by pathological examination; (2) having no cancerous thrombus found in the portal vein (main trunk or two major branches), hepatic veins, or bile duct; and (3) having no extrahepatic metastasis found. Tumor differentiation was defined according to the Edmondson grading system. Tumor staging was defined according to the 6th edition of tumor-node-metastasis (TNM) classification of Unio Internationale Contra Cancrum. HCC staging was defined according to the Barcelona Clinic Liver Cancer (BCLC) staging system. The clinicopathologic characteristics of 90 patients were summarized in Supplementary Table 1.

All patients were followed up every 2 months during the first post-operative year and at least every 3–4 months afterward. Follow-up was finished on March 31, 2011. Most patients died of intrahepatic recurrence, distal metastasis, or complicated liver cirrhosis. All patients were monitored prospectively by serum AFP, abdomen ultrasonography (US), and chest X-ray every 1–6 months, according to the postoperative time. For patients with test results suggestive of recurrence, computed tomography (CT) and/or magnetic resonance imaging (MRI) were used to verify whether intrahepatic recurrence and/or distal metastasis had occurred. A diagnosis of recurrence was based on typical imaging appearance in CT and/or MRI scan and an elevated AFP level. Overall survival (OS) was defined as the interval between surgery and either death or the last observation taken. Time to recurrence (TTR) was measured from the date of resection until either detection of recurrent tumor or the last follow-up assessment. The current study was approved by the Institutional Ethics Committee of Zhongshan Hospital, Fudan University. All patients provided written informed consent.

2.2. Cells and reagents

Purified pcDNA3.1-UCH37 plasmid was obtained as a kind gift from Professor Xingzhong Wu (Department of Biochemistry, Shanghai Medical School, Fudan University). L02 and Huh7 cell lines were purchased from the Type Culture Collection of Chinese Academy of Sciences (Shanghai, China); supervision anti-rabbit or anti-mouse detection reagents (HRP), from Kangwei Biotechnology (Beijing, China); mouse anti-UCH37 antibody, mouse anti-PRP19 antibody and mouse anti-Ub antibody, from Santa Cruz Biotechnology (Santa Cruz, CA, USA); rabbit anti-PRP19 antibody, from Abcam Biotechnology (USA); mouse anti-Flag and anti-GAPDH antibodies, from Kangwei Biotechnology (Beijing, China); ECL Western Blotting Substrate System, from Pierce (Rockford, IL, USA); Lipofectamine 2000 and FITC-AnnexinV/propidium iodide (PI) cell apoptosis kit, from Invitrogen (USA); Transwell with 8-μm pore polycarbonate membrane, from Millipore (USA); crystal violet, from Sigma (St. Louis, USA); Matrigel, from BD Biosciences (USA); MG132, from Merck (Germany); and cycloheximide, from Beyotime Biotechnology (Shanghai, China).

2.3. Cell culture and stable transfectants

Respectively, L02 and Huh7 cells were cultured in RPMI medium 1640 (Thermo, USA) and DMEM (Thermo, USA), supplemented with 15% fetal bovine serum (FBS) (GIBCO, Austria) at 37 °C in a humidified atmosphere containing 5% CO_2. The cell line stably expressing UCH37 was generated by the retroviral infection of L02 cells. The target sequence for the small hairpin RNA (shRNA) for UCH37 is 5′-CCTGTTAATGGGAGACTGTAT-3′. A retrovirus-expressing shRNA specific to UCH37 was infected into Huh7 cells. Briefly, a retroviral vector containing either human UCH37 cDNA with an N-terminal Flag-tag or a specific shRNA, pHCMV-G and pCMV-dR8.9 were co-transfected into 293 T cells, and the viral supernatants were collected to infect L02 or Huh7 cells. Monoclonal cells were then selected, cloned, and screened for UCH37 over-expression or down-regulation.

2.4. Real-time quantitative PCR analysis

The mRNA quantity of specific genes, calculated using the ΔΔCt method, was normalized against β-actin. Real-time PCR amplification involved the use of an ABI Prism 7500 sequence detector (Applied Biosystems) and SYBR reagent (Takara, Japan). All the measurements

were performed in triplicate. The sequences of the primer pairs were as follows:

UCH37: 5′-GTGGTTCAGGACTCCCGACTT-3′ and 5′-GCTGTCTGG CGAAACTGTTGT-3′;
PRP19: 5′-AAGGCCATACCAAGAAGGTCACCA-3′ and 5′-ACCGACC AAATCCTGATAGTGGCA-3′;
β-Actin: 5′-AGCGAGCATCCCCCAAAGTT-3′ and 5′-GGGCACGAA GGCTCATCATT-3′.

2.5. Western blotting (WB)

The cells were lysed in lysis buffer (20 mM Tris–HCl, pH 7.5, 150 mM NaCl, 1 mM EDTA, and 1% Triton X-100 with protease inhibitor), and their extracts were clarified via centrifugation. The cell-lysated proteins were separated on 12% SDS-PAGE gel and then transferred to nitrocellulose membrane (Amersham Biosciences, Piscataway, NJ). The membranes were blocked in blocking solution [50 mM Tri–HCl, 150 mM NaCl, 5% (w/v) non-fat dry milk and 0.1% Tween-20] at room temperature for 1 h, followed by incubation with appropriate primary antibodies at 4 °C overnight. After incubating with appropriate secondary antibodies at room temperature for 1 h, the blots were demonstrated by enzyme-linked chemiluminescence performed using a LAS3000 imaging system (FUJI, Japan).

2.6. Co-immunoprecipitation (co-IP)

The cell-lysated proteins were precleared with 2 μg appropriate antibodies at 4 °C for 8 h, and then incubated with protein A-agarose (Roche) and antibodies at 4 °C overnight. For co-IP experiments using anti-Ub antibody, the cell lysates contained 1% SDS and received prior heat treatment. The precipitates were pelleted, washed three times with the lysis buffer and analyzed by western blotting.

2.7. Immunohistochemistry

Five-micron thick sections of formalin-fixed and paraffin-embedded tissues were deparaffinized and rehydrated, followed by high-temperature antigen retrieval via microwave in 0.1 M citrate solution (pH 6.0) for 15 min. After blocked in 5% normal goat serum at room temperature for 30 min, the sections were incubated with the mouse anti-UCH37 antibody at 4 °C overnight, then incubated with biotinylated secondary antibody at room temperature for 30 min, and finally immunostained by the avidin–biotin complex (ABC) technique using 3,3′-diaminobenzidine (DAB). Hematoxylin was used as a counterstain.

The interpretation of immunoreactivity was performed in a semi-quantitative manner by analyzing the extent and intensity of staining positivity of cells. Interpretation scores were as follows: 0, ≤5% cell positivity or negative staining; +1, 6%–20% cell positivity or mild staining; +2, 21%–50% cell positivity or moderate staining; and +3, ≥50% cell positivity or intense staining. Final scores, product of the scores mentioned earlier, greater than 2 were considered positive. Staining was evaluated independently by two pathologists and any discrepancy was resolved by consensus review.

2.8. Immunofluorescence staining and confocal laser scanning microscopy

At the confluence by 60%, the cells were plated onto sterilized glass coverslips, which were to be washed in phosphate-buffered saline (PBS) and fixed in acetone/carbinol (V/V = 1/1) on ice for 2 min. The slides were then blocked in PBS plus 5% FBS at 37 °C for 1 h, followed by an incubation with anti-UCH37/anti-Flag and anti-PRP19 antibodies at 4 °C overnight. After that, the slides were washed three times with PBS-T (PBS plus 0.2% Triton X-100). For double immunofluorescence staining, the slides were incubated with rhodamine-conjugated anti-mouse IgG and fluorescein isothiocyanate (FITC)-conjugated anti-rabbit IgG at 37 °C for 1 h. The slides were then stained briefly with DAPI, washed with PBS-T, mounted, and analyzed via the confocal laser scanning microscope (Leica TCS SP5, Germany).

2.9. In vitro cell apoptosis assay

UCH37 overexpressing/silencing cells and the control cells were stained with FITC-AnnexinV and PI, and then evaluated for apoptosis by flow cytometry according to the manufacturer's protocol (Invitrogen, USA). Briefly, cells were harvested after the incubation period, washed twice in cold PBS, and centrifuged at 1000 rpm for 5 min. About 1×10^6 cells were re-suspended in 100 μl 1× annexin-binding buffer and transferred to a sterile flow cytometry glass tube. 5 μl FITC-AnnexinV and 1 μl 100 μg/ml PI were added to each tube, followed by incubation at room temperature for 15 min in the dark. After the incubation period, 400 μl 1× annexin-binding buffer was added to each tube and samples were analyzed by flow cytometry (Epics Altra, Beckman, USA).

2.10. In vitro cell cycle distribution assay

UCH37 overexpressing/silencing cells and the control cells were harvested, washed twice in cold PBS, and then fixed in 70% ethanol at 4 °C overnight. After centrifugation, the cell pellets were re-suspended in 1 ml PBS with 100 μg/ml RNase A, 50 μg/ml PI and 0.2% Triton X-100, followed by incubation at 4 °C for 30 min in the dark. After that, cell cycle distribution was analyzed by flow cytometry (Epics Altra, Beckman, USA).

2.11. Scratch-wound assay

Cells were seeded in six-well dishes at a density of 5×10^5 cells per well and grown to be confluent. The cell monolayers were scraped with a sterile blue micropipette tip to create a denuded area of constant width. Cells were washed with PBS to remove cell debris, and then cultured in medium with 15% FBS. The wound closure was monitored and photographed at 48 h after wounding.

2.12. Transwell migration and invasion assays

Cells were harvested and suspended in the serum free medium supplemented with 1% BSA. For transwell migration assays, cell suspensions were loaded into the top chamber with a non-coated membrane at a concentration of 2×10^4 cells/100 μl. For transwell invasion assays, cell suspensions were loaded into the top chamber with a Matrigel-coated membrane at a concentration of 1×10^5 cells/100 μl. In both assays, medium containing 15% FBS was used as a chemoattractant in the lower chamber. After incubation for 48 h, cells that had migrated or invaded to the lower surface of the filter were fixed with 4% paraformaldehyde, followed by stained with 0.1% crystal violet. Cells were counted in four independent fields with light microscope.

2.13. RNA interference

At the confluence by 70%, the L02-UCH37 cells were transfected with either PRP19 small interfering RNA (siRNA) or control siRNA using Lipofectamine 2000 according to the manufacturer's instructions (Invitrogen, USA). Final concentration of siRNA when added to the cells was 40 nM. The expression of PRP19 was assessed by immunoblotting after transfection. At 48 h post-transfection, cells were used for scratch-wound assay, or harvested for transwell migration and invasion assays. The siRNA duplex oligoribonucleotides were

synthesized in GenePharma Biotechnology (Shanghai, China), and the sequences were as follows:

PRP19 siRNA-1: 5′-GGCUCAUCGAGAAGUACAUTT-3′ (sense) and 5′-AUGUACUUCUCGAUGAGCCTT-3′ (anti-sense);
PRP19 siRNA-2: 5′-GCCACUAUCAGGAUUUGGUTT-3′ (sense) and 5′-ACCAAAUCCUGAUAGUGGCTT-3′ (anti-sense);
PRP19 siRNA-3: 5′-GCCAAGUUCAUCGCUUCAATT-3′ (sense) and 5′-UUGAAGCGAUGAACUUGGCTT-3′ (anti-sense);
Control: 5′-UUCUCCGAACGUGUCACGUTT-3′ (sense) and 5′-ACGUGACACGUUCGGAGAATT-3′ (anti-sense).

2.14. Protein extraction and preparation for Isobaric Tag for Relative and Absolute Quantitation (iTRAQ)

The cells were lysed in lysis buffer (20 mM Tris–HCl, pH 7.5, 150 mM NaCl, 1 mM EDTA, and 1% Triton X-100 with protease inhibitor) and sonicated, and the supernatant was collected by centrifugation at 30,000 *g* for 15 min. After treated with acetone, the cell extracts were resuspended in 250 mM triethylammonium bicarbonate (TEAB), followed by incubation with 10 mM DL-dithiothreitol (DTT) in water bath at 56 °C for 1 h, and then with 55 mM iodoacetamide (IAM) in darkroom at room temperature for 45 min. The proteins (100 μg each) were digested with trypsin at 37 °C for 16 h. Subsequently, the peptides were dried with vacuum centrifuge and resuspended in 500 mM TEAB for further iTRAQ labeling. The protein concentration was determined using Bradford assay.

2.15. iTRAQ labeling and strong cation exchange (SCX) separation

The iTRAQ labeling of tryptic peptides was performed using iTRAQ reagent Multiplex kit (Applied Biosystems, Foster City, CA) according to the manufacturer's protocol. The peptides labeled with respective isobaric tags were incubated at room temperature for 2 h and vacuum centrifuged to dryness. Then the iTRAQ labeled peptides samples were reconstituted in Buffer A [25 mM NaH_2PO_4, 25% acetonitrile (ACN), pH 2.7] and fractionated using Ultremex SCX column (250 × 4.6 mm, 5 μm particle size, 200 Å pore size) via LC-20AB HPLC Pump system (Shimadzu, Japan) at flow rate 1.0 ml/min. The 35 min HPLC gradient consisted of 100% Buffer A for 10 min; 5–35% Buffer B (25 mM NaH_2PO_4, 25% ACN, 1 M KCl, pH 2.7) for 11 min; 35–80% Buffer B for 1 min; 80% Buffer B for 3 min and 100% Buffer

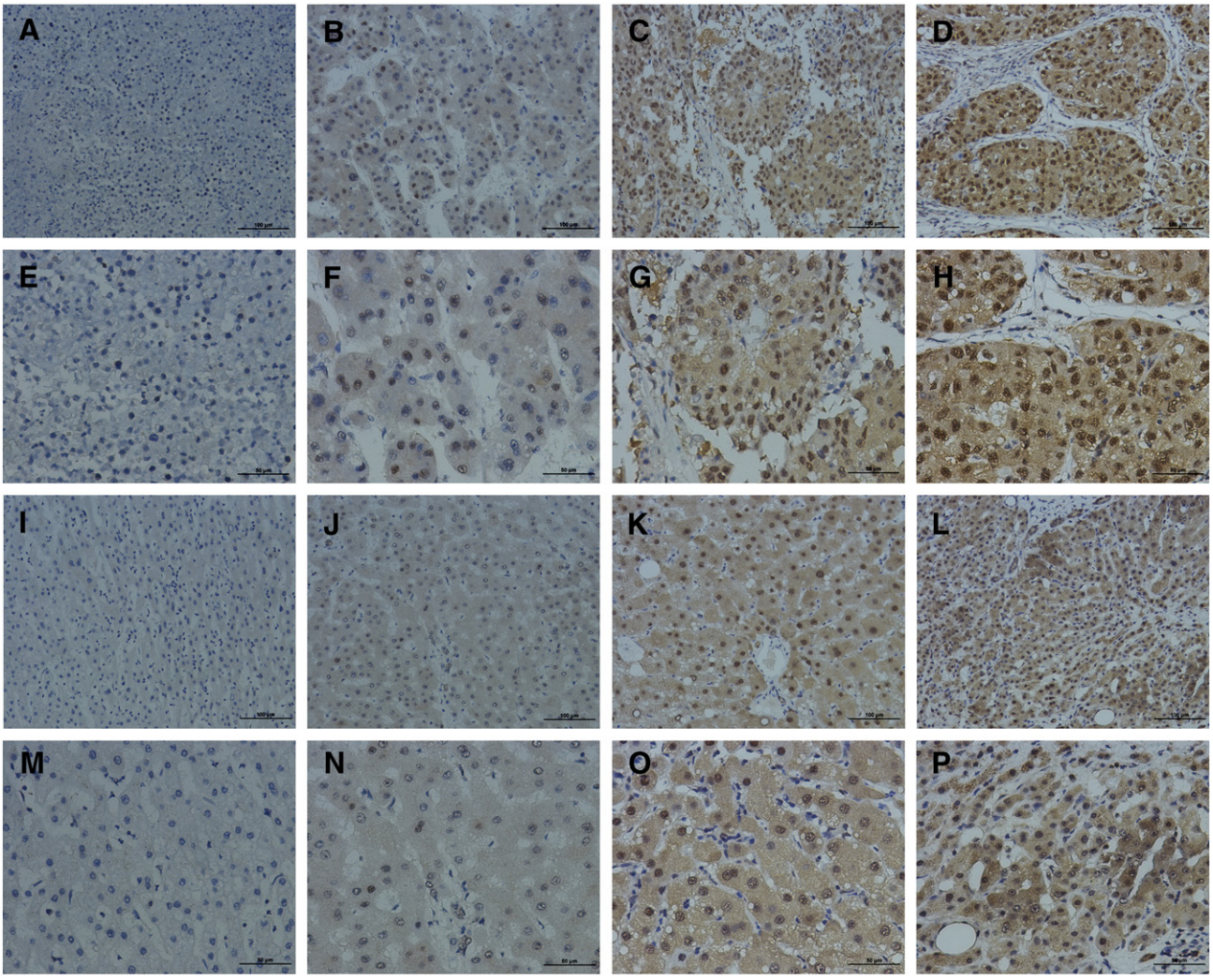

Fig. 1. Typical patterns of UCH37 staining in HCC tissues and para-cancerous tissues. (A and E) HCC tissue, negative staining; (B and F) HCC tissue, mild staining; (C and G) HCC tissue, moderate staining; (D and H) HCC tissue, intense staining; (I and M) para-cancerous tissue, negative staining; (J and N) para-cancerous tissue, mild staining; (K and O) para-cancerous tissue, moderate staining; and (L and P) para-cancerous tissue, intense staining. The magnification was 200 (A–D, I–L) and 400 (E–H, M–P).

Table 1
Univariate analyses of factors associated with survival and recurrence.

Variables	OS		TTR	
	Hazard ratio (95% CI)	*p*	Hazard ratio (95% CI)	*p*
Sex (male vs. female)	1.423 (0.606–3.346)	0.418	1.025 (0.505–2.084)	0.945
Age, y (>52 vs. ≤52)	1.034 (0.592–1.804)	0.906	0.895 (0.539–1.487)	0.670
HBsAg (negative vs. positive)	0.915 (0.362–2.312)	0.851	0.651 (0.294–1.440)	0.289
HCV (positive vs. negative)	1.039 (0.142–7.583)	0.970	2.001 (0.486–8.241)	0.337
BCLC stage (stage B/C vs. A)	4.337 (1.557–12.086)	**0.005**	1.796 (0.933–3.459)	0.080
Liver cirrhosis (yes vs. no)	1.813 (0.563–5.840)	0.319	2.195 (0.795–6.062)	0.129
ALT, units/L (>75 vs. ≤75)	1.295 (0.608–2.761)	0.502	1.303 (0.658–2.578)	0.448
AFP, ng/mL (>20 vs. ≤20)	2.148 (1.180–3.910)	**0.012**	1.464 (0.873–2.454)	0.149
Tumor differentiation (III–IV vs. I–II)	0.848 (0.264–2.731)	0.783	1.409 (0.563–3.524)	0.464
Tumor encapsulation (complete vs. none)	0.633 (0.341–1.176)	0.148	0.516 (0.291–0.914)	**0.023**
Tumor size, cm (>5 vs. ≤5)	2.506 (1.279–4.912)	**0.007**	1.841 (1.058–3.204)	**0.031**
Tumor number (multiple vs. single)	0.998 (0.521–1.913)	0.996	1.041 (0.573–1.893)	0.894
TNM stage (II–III vs. I)	2.184 (1.225–3.892)	**0.008**	1.984 (1.187–3.317)	**0.009**
Vascular invasion (yes vs. no)	2.471 (1.411–4.328)	**0.002**	2.196 (1.318–3.659)	**0.003**
$UCH37_{HCC-para-HCC}$ (≥2 vs. <2)[a]	1.661 (0.941–2.931)	0.080	2.087 (1.232–3.536)	**0.006**

Bold items have been considered statistically significant.
Note: Cox proportional hazards regression model was used in univariate analysis.
Abbreviations: 95% CI, 95% confidence interval; HBsAg, hepatitis B surface antigen; HCV, hepatitis C virus; and ALT, alanine aminotransferase.
[a] $UCH37_{HCC-para-HCC}$: The extra part from the score of the HCC tissue minus that of the para-cancerous tissue, according to the criterion for immunohistochemistry.

A for 10 min. The chromatograms were recorded at 214 nm. The collected fractions were desalted using Strata X C18 column (Phenomenex), vacuum centrifuged and reconstituted in 0.1% formic acid (FA) for subsequent LC–MS/MS analysis.

2.16. LC–MS/MS analysis

The mass spectroscopy (MS) analysis was performed using an LTQ-Orbitrap XL mass spectrometer (Thermo Scientific, San Jose, CA, USA), coupled with online micro flow HPLC system (Shimadzu, Japan). The concentration of each SCX fraction dissolved in 0.1% FA was diluted to 0.5 μg/μl. For each sample, 10 μl solution was loaded onto a 200-μm internal diameter × 2-cm-length C18 trap column with 100% Buffer C (2% ACN, 0.1% FA) at 15 μl/min for 10 min, and then the peptides were separated using a 75-μm internal diameter × 10-cm-length analytical C18 PicoFrit column. The peptides were eluted at a flow rate of 400 nl/min across the separation column with a linear gradient of 2–35% Buffer D (98% ACN, 0.1% FA) for 44 min, 35–80% Buffer D for 2 min, maintenance in 80% Buffer D for 4 min, and then returning to 2% Buffer D within 1 min. The LTQ-Orbitrap XL was operated in a data-independent mode automatically switching between MS, MS/MS and higher-energy collision dissociation (HCD) using a threshold of 30,000 for ion selection. The mass spectrometer data was acquired in the positive ion mode with a selected mass range of 350–2000 m/z.

2.17. Protein identification and database search

The data acquisition was performed with Xcalibur 2.1 software (Thermo Fisher) and the proteins were identified and quantified using Mascot search engine (Matrix Science, London, U.K.; version 2.3.2) with the Mascot Daemon program (Matrix Science; version 2.3.2). The defined parameters were as follows: (1) Type of search, MS/MS Ion search; (2) Enzyme, Trypsin; (3) Peptide Mass Tolerance, 10 ppm; (4) Fragment Mass Tolerance, ±0.05 Da; (5) Fixed modifications, Carbamidomethyl (C); (6) Variable modifications, Gln → pyro-Glu (N-term Q) and Oxidation (M); (7) Max Missed Cleavages, 1; and (8) Database, IPI_human, (total sequences, 89,378; total residues, 35,817,989).

The proteins were identified with at least one unique peptide. Following identification, those with a minimum of two unique peptides were used for further quantification analysis. The differentially expressed proteins were defined as the expression ratio of >1.50 or <0.67 compared with the control. Furthermore, the differentially expressed proteins were categorized using Gene Ontology (GO)

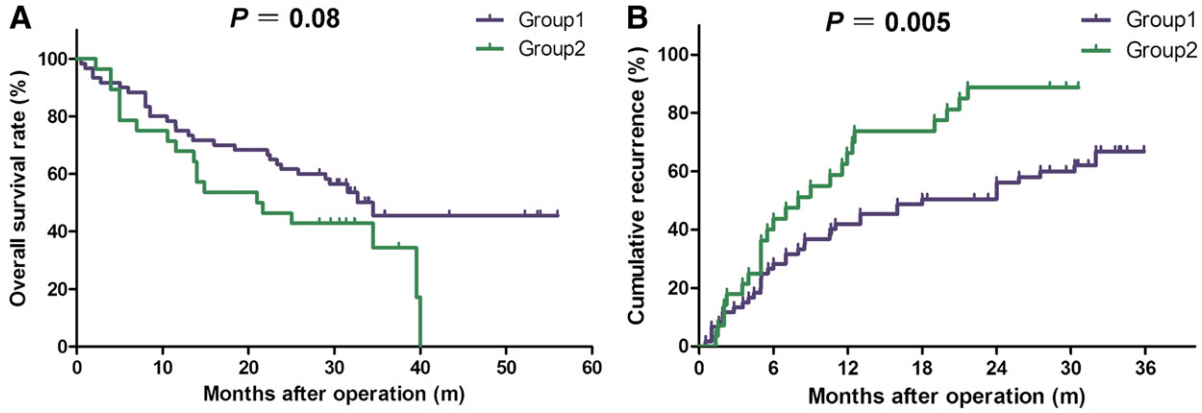

Fig. 2. The prognostic significance was assessed using Kaplan–Meier survival estimate and log-rank test. Comparison of OS (A) and TTR (B) by UCH37 expression. According to the criterion for immunohistochemistry, Group 1, the patient whose extra part from the score of the HCC tissue minus that of the para-cancerous tissue was less than 2; and Group 2, the patient whose extra part from the score of the HCC tissue minus that of the para-cancerous tissue was greater than or equal to 2.

information (http://www.geneontology.org/) [23] and evaluated using the Kyoto Encyclopedia of Genes and Genomes (KEGG) pathways database [24].

2.18. Statistical analysis

All values were expressed as mean ± standard deviation (SD). Statistical analyses were done by SPSS 16.0 for Windows (SPSS). The χ^2 test, Fisher's exact test, and Student's *t* test were used for comparison between groups. Cumulative survival time and cumulative recurrence rate were calculated by the Kaplan–Meier method and analyzed by the log-rank test. Univariate and multivariate analyses were based on the Cox proportional hazard regression model. $p<0.05$ was considered statistically significant.

3. Results

3.1. UCH37 expression in HCC patients and factors associated with prognosis

Immunostaining for UCH37 was assessed in the cancerous tissues and the adjacent non-cancerous liver tissues in 90 cases of human HCC (Fig. 1). The percentage of UCH37 positivity in the cancerous tissues was significantly higher than that in the para-cancerous tissues [92.2% (83/90) vs. 74.4% (67/90), respectively, $p=0.001$]. Among 61 recurrence patients, we found out the similar result [92.2% (55/61) positive in HCC vs. 70.5% (43/61) in para-cancerous tissues, respectively, $p=0.006$]. The paired *t* test showed that the expression of UCH37 in the cancerous tissues was significantly higher than that in the adjacent para-cancerous tissues ($p<0.001$), which was also found among 61 recurrence patients ($p<0.001$).

Univariate analysis showed that tumor size, TNM stage and vascular invasion were unfavorable predictors for OS and TTR. AFP level and BCLC stage were associated with OS, and encapsulation was associated with TTR (Table 1). Meanwhile, UCH37 was found to be prognostic for TTR ($p=0.006$, Table 1), but not for OS ($p=0.08$, Table 1, Fig. 2A). The patient, whose extra part from the score of the HCC tissue minus that of the para-cancerous tissue was greater than or equal to 2, had a higher cumulative risk of developing HCC recurrence after resection (Fig. 2B). Multivariate analysis indicated that UCH37 was an independent prognosticator for TTR ($p=0.004$, Table 2). However, UCH37 expression was not related with other clinicopathologic characteristics (Table 3).

Table 2
Multivariate analyses of factors associated with OS and TTR.

	Hazard ratio (95% CI)	*p*
OS[a]		
BCLC stage (stage B/C vs. A)	2.557 (0.758–8.625)	0.130
AFP, ng/mL (>20 vs. ≤20)	1.968 (1.054–3.675)	**0.034**
Tumor size, cm (>5 vs. ≤5)	1.567 (0.717–3.424)	0.260
TNM stage (II–III vs. I)	1.292 (0.681–2.449)	0.433
Vascular invasion (yes vs. no)	1.779 (0.973–3.253)	0.062
TTR[b]		
Tumor encapsulation (complete vs. none)	0.616 (0.336–1.126)	0.116
Tumor size, cm (>5 vs. ≤5)	2.072 (1.118–3.841)	**0.021**
TNM stage (II–III vs. I)	1.326 (0.758–2.319)	0.323
Vascular invasion (yes vs. no)	1.648 (0.960–2.828)	0.070
$UCH37_{HCC-para-HCC}$ (≥2 vs. <2)[c]	2.449 (1.378–4.351)	**0.002**

Note: Multivariate analysis and Cox proportional hazards regression model were used. Variables were adopted for their prognostic significance by univariate analysis ($p<0.05$).

[a] BCLC stage, AFP, tumor size, TNM stage and vascular invasion were included in multivariate analysis for OS.

[b] Tumor encapsulation, tumor size, TNM stage, vascular invasion and UCH37 expression were included in multivariate analysis for TTR.

[c] $UCH37_{HCC-para-HCC}$: The extra part from the score of the HCC tissue minus that of the para-cancerous tissue, according to the criterion for immunohistochemistry.

Table 3
Correlation between UCH37 and other clinicopathologic characteristics.

	$UCH37_{HCC-para-HCC}$		
	<2	≥2	*p*
Patients	61	29	
Sex			
Female	8	5	0.842
Male	53	24	
Age, y			
≤52	31	18	0.317
>52	30	11	
HBsAg			
Negative	4	5	0.229
Positive	57	24	
HCV			
Negative	61	27	0.101*
Positive	0	2	
ALT, units/L			
≤75	51	26	0.658
>75	10	3	
Preoperative AFP, ng/mL			
≤20	28	9	0.180
>20	33	20	
Liver cirrhosis			
No	5	4	0.652
Yes	56	25	
BCLC stage			
A	11	7	0.499
B/C	50	22	
Tumor size			
≤5 cm	18	12	0.264
>5 cm	43	17	
Tumor number			
Single	46	23	0.683
Multiple	15	6	
Tumor encapsulation			
No	39	21	0.425
Complete	22	8	
Vascular invasion			
No	36	17	0.972
Yes	25	12	
TNM stage			
I	30	13	0.699
II–III	31	16	
Tumor differentiation			
I–II	58	26	0.335
III–IV	3	3	

* Fisher's exact tests; χ^2 tests for all the other analyses.

3.2. Establishment of stable monoclonal cell lines

To explore the biological roles of UCH37 in HCC, we established stable monoclonal cell lines by altering the UCH37 expression level. The treated monoclonal L02 cells stably expressing the Flag–UCH37 fusion protein were performed (Fig. 3A, C). Meanwhile, we infected a retrovirus-expressing shRNA specific to UCH37 into Huh7 cells and generated stable monoclonal UCH37-knockdown Huh7 cells (Fig. 3B, D).

3.3. UCH37 does not affect cell apoptosis and cell cycle distribution in HCC cells

To evaluate the effect on apoptosis of UCH37 in HCC cells, the presence of apoptotic cells was determined by the application of double staining with FITC-Annexin V and PI. Early apoptotic cells were represented as FITC-positive and PI-negative, and late apoptotic cells as FITC-positive and PI-positive. Consequently, no significant difference was found in the apoptotic cell fraction between the UCH37 overexpressing/silencing cells and the control cells (Fig. 4A, B). We also analyzed the cell cycle distribution of the stable cell lines by flow cytometry after PI staining. The results showed that the cell cycle

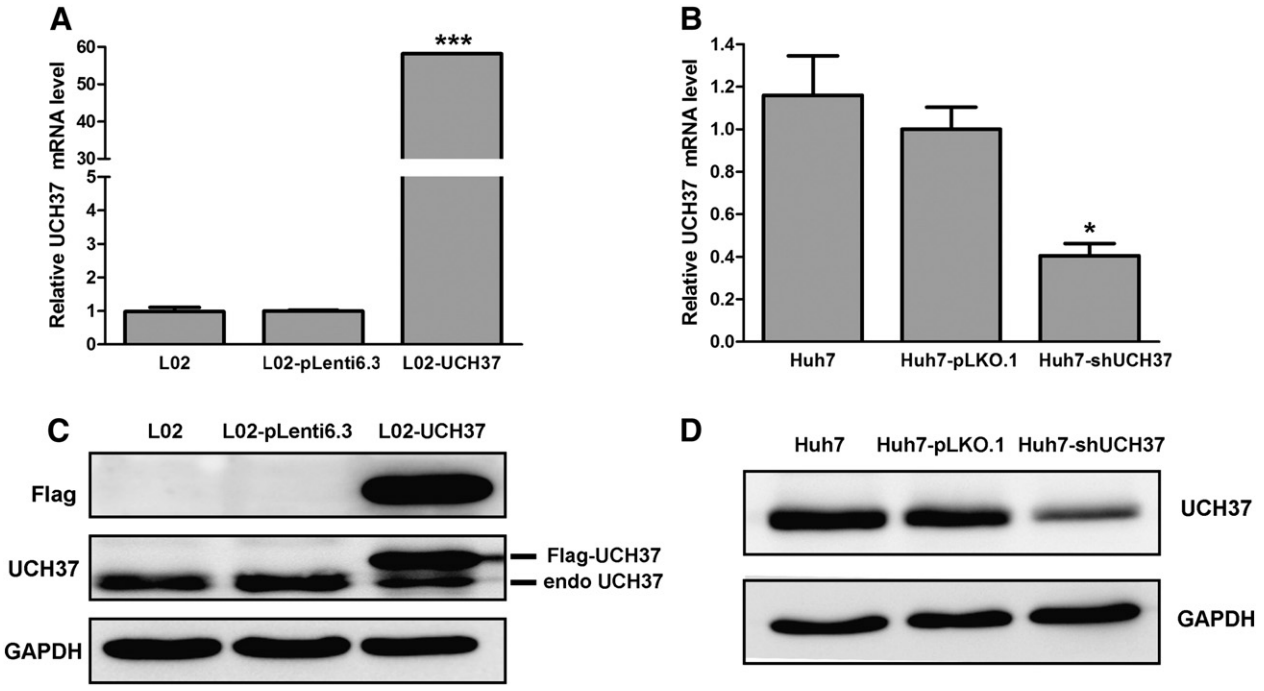

Fig. 3. Establishment of stable monoclonal cell lines. The mRNA level of UCH37 was assessed in the treated L02 (A) or Huh7 (B) cells. Real-time PCR of β-actin mRNA expression was performed as a control. Data were presented as mean value ± standard deviation (SD). * $p<0.05$, *** $p<0.001$. The protein level of UCH37 was assessed in the treated L02 (C) or Huh7 (D) cells. GAPDH was used as a loading control. L02-pLenti6.3, L02 cells carrying an empty vector; L02-UCH37, the monoclonal L02 cells stably expressing Flag-UCH37 fusion protein; Huh7-pLKO.1, Huh7 cells carrying an empty vector; and Huh7-shUCH37, the stable monoclonal Huh7 cells whose UCH37 expression was down-regulated.

distribution did not present any distinguishable differences in the UCH37 overexpressing/silencing cells, compared with the control cells (Fig. 4C, D).

3.4. UCH37 promotes cell migration and invasion

Since metastasis and recurrence represent the main deleterious characteristic of HCC, we determined the migratory and invasive potential of the treated cell lines. In the scratch assay, the treated L02 cells stably expressing the Flag–UCH37 fusion protein migrated into the wound area and organized a dense cellular network, resulting in nearly complete wound recovery after 48 h, while migration into the wound area of Huh7-shUCH37 cells was significantly inhibited (Fig. 5A, B).

In the transwell migration assay, the migrated cells increased from 98 ± 10 cells per field for control to 183 ± 16 cells per field for L02-UCH37 cells ($p<0.01$) (Fig. 5C). The migrated cells in control cells and Huh7-shUCH37 cells were, respectively, 97 ± 4 cells and 28 ± 4 cells ($p<0.001$) (Fig. 5D). In the transwell invasion assay, we found out the similar results. UCH37-knockdown reduced the cell capability to invade extracellular matrix (Huh7-pLKO.1, 23 ± 3 vs. Huh7-shUCH37, 3 ± 1, $p<0.05$), whereas forced expression of UCH37 increased invasiveness (L02-pLenti6.3, 14 ± 2 vs. L02-UCH37, 51 ± 2, $p<0.001$) (Fig. 5E, F). These data indicated that UCH37 promoted migratory and invasive abilities in vitro, and demonstrated that reducing UCH37 expression level attenuated HCC cell aggressiveness.

3.5. Identification of differentially expressed proteins using iTRAQ

To determine differentially expressed proteins that may serve as potential interaction targets of UCH37, total proteins, extracted from the treated L02 cells stably expressing the Flag–UCH37 fusion protein and the L02 cells carrying an empty vector, were analyzed using iTRAQ experiments. In total, 2134 proteins (7225 unique peptides) were confidently identified, of which 1680 proteins were used for further quantification analysis. Using the criteria described in the "Material and methods", 19 proteins were found to be up-regulated and 21 down-regulated in the treated L02 cells, compared with the control cells (Table 4).

3.6. Functional classification and pathway analysis of differentially expressed proteins

In order to understand the biological impact of UCH37, the differentially expressed proteins identified by iTRAQ were imported into the Gene Ontology (GO) database (http://www.geneontology.org/) and the Kyoto Encyclopedia of Genes and Genomes (KEGG) pathways database. For GO analysis, the proteins were categorized based on cellular component, molecular function or biological process. As a result, the proteins appeared to be distributed all over the cell (Supplementary Table 2). The top six molecular functions included protein binding, catalytic activity, nucleic acid binding, transcription regulator activity, enzyme regulator activity and transferase activity (Supplementary Table 3). In addition, the proteins were found to participate in a variety of important biological processes including metabolic, immune, response to stimulus, cellular, and transport-related processes (Supplementary Table 4). For KEGG pathways analysis, the proteins covered 55 KEGG pathways, including spliceosome, focal adhesion, metabolism, endocytosis, antigen processing and presentation, MAPK signaling pathway, TGF-β signaling pathway and Wnt signaling pathway (Supplementary Tables 5–7).

3.7. UCH37 deubiquitinates PRP19 and interacts with PRP19

We selected some of the up-regulated proteins for immunoblot analysis (Supplementary Fig. 2). Although the direction of the change as detected by iTRAQ was consistent with the immunoblot analysis, there was some degree of difference between the two techniques. These differences observed between the two techniques could be

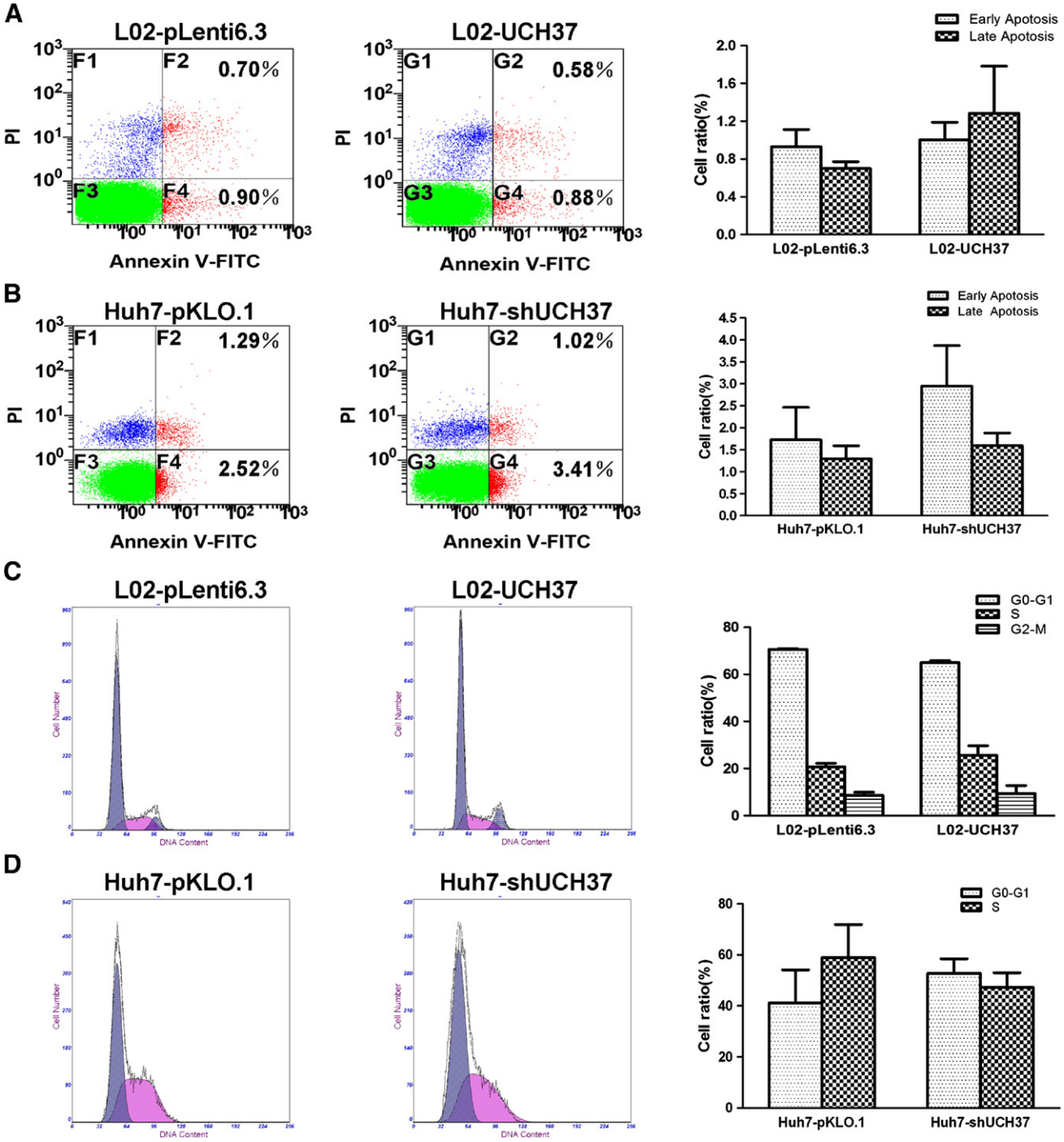

Fig. 4. UCH37 does not affect cell apoptosis and cell cycle distribution in HCC cells. Cell apoptosis was assessed by double staining of FITC-AnnexinV/PI and subsequently flow cytometry (A and B). The patterns shown are representative of three separate experiments (left and middle). The percentages of early apoptotic cells and late apoptotic cells were counted (right). Cell cycle distribution was analyzed by flow cytometry after PI staining (C and D). The patterns shown are representative of three separate experiments (left and middle). The percentages of cells in each phase were counted (right). Columns represented the mean of three independent experiments; bars, SD; L02-pLenti6.3, L02 cells carrying an empty vector; L02-UCH37, the monoclonal L02 cells stably expressing Flag-UCH37 fusion protein; Huh7-pLKO.1, Huh7 cells carrying an empty vector; and Huh7-shUCH37, the stable monoclonal UCH37-knockdown Huh7 cells.

attributed to factors such as the potency of antibodies, differences inherent in each technical approach, and/or some other uncertainties. Consequently, PRP19 was chosen for further study, because PRP19 was consistently significantly up-regulated in L02-UCH37 cells compared with the control cells using both techniques.

Although the protein level of PRP19 was increased in L02-UCH37 cells, compared with the control cells (Fig. 6A), the mRNA level of PRP19 presented no significant difference between the two cells (Fig. 6B). To investigate whether the degradation of PRP19 was mediated through ubiquitin proteasome pathway (UPP), L02 cells were treated with proteasome inhibitor MG132 (10 μmol/L) for 24 h. Our results indicated that the addition of MG132 induced accumulation of PRP19 (Fig. 6C). Furthermore, to investigate whether PRP19 was one of UCH37 substrates, the level of ubiquitinated PRP19 was assessed. Co-immunoprecipitation (co-IP) assay indicated that when the expression of PRP19 was the same in both cells, the level of

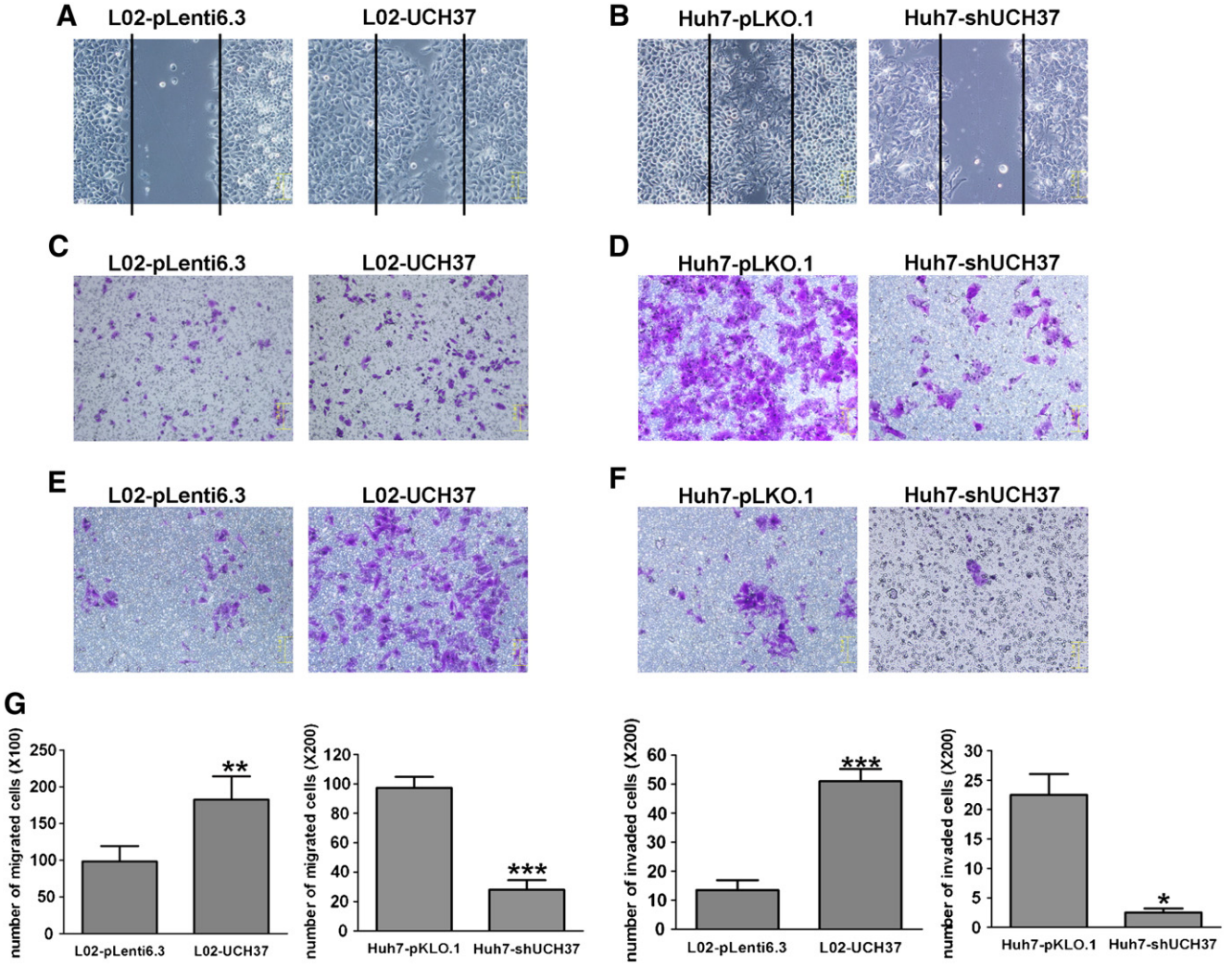

Fig. 5. UCH37 promotes cell migration and invasion. (A and B) Representative images at 48 h after wounding were shown. (C and D) Cells were seeded in the top chamber with a non-coated membrane and allowed to migrate for 48 h. (E and F) Cells were seeded in the top chamber with a Matrigel-coated membrane and allowed to invade for 48 h. Migrated or invaded cells were stained by crystal violet. Representative images of three independent experiments were shown. The magnification was 100 (C) and 200 (A, B, D, E and F). (G) The number of migrated or invaded cells was manually counted in four independent fields per well with light microscope. Columns represented the average of four random fields; bars, SD; L02-pLenti6.3, L02 cells carrying an empty vector; L02-UCH37, the monoclonal L02 cells stably expressing Flag-UCH37 fusion protein; Huh7-pLKO.1, Huh7 cells carrying an empty vector; Huh7-shUCH37, the stable monoclonal UCH37-knockdown Huh7 cells. * $p<0.05$, ** $p<0.01$, *** $p<0.001$.

ubiquitinated PRP19 was significantly decreased in L02-UCH37 cells compared with the control cells (Fig. 6D).

However, immunoblot analysis showed that the expression of PRP19 did not present any significant change in the monoclonal UCH37-knockdown Huh7 cells, compared with Huh7 cells carrying an empty vector (Fig. 6E). Then, the expression of PRP19 from the control cells and Huh7-shUCH37 cells treated with 20 μM cycloheximide for different time intervals was analyzed by western blotting. The results showed that the silencing of UCH37 revealed an increased rate of degradation of PRP19, indicating the physiological relevance of UCH37 in regulating PRP19 (Fig. 6F).

Subsequently, the possibility that UCH37 could interact with PRP19 was confirmed by co-IP and confocal laser scanning microscopy analysis. Consequently, in L02-UCH37 cells, PRP19 was easy to be detected through anti-PRP19 antibody in the Flag-immunoprecipitates (Fig. 7A). Reciprocal co-IP experiments using anti-PRP19 antibody indicated the existence of Flag and UCH37, as confirmed by immunoblotting (Fig. 7B). To verify the stringency of co-IP, parallel experiments were done in which co-IP antibody was replaced with isotype control antibody or PBS. Meanwhile, control experiments showed that PRP19 was exactly associated with UCH37, but not with Flag (Supplementary Fig. 3). This interaction of UCH37 with PRP19 with endogenously UCH37 was confirmed in Huh7 cells (Fig. 7C, D).

Furthermore, the localizations of UCH37 and PRP19 were visualized under confocal laser scanning microscopy. The L02-UCH37 cells expressing the Flag–UCH37 fusion protein exhibited fluorescence concentrated in the cytoplasm, and also in the nucleus. PRP19 was found to be mainly localized in the nucleus. Co-localization of two proteins in the nucleus was evidenced by overlapping fluorescence signals (Fig. 7E, F). While in the Huh7 cells, the distribution of PRP19 was diffuse — nucleus and cytoplasm as did UCH37. Overlapping fluorescence signals showed that two proteins were co-localized mainly in the nucleus, and also a little in the cytoplasm (Fig. 7G).

3.8. PRP19 is involved in UCH37-induced HCC cell migration and invasion

To investigate the relationship between UCH37, PRP19 and the capability of cell migration and invasion, the expression of PRP19 in L02-UCH37 cells was down-regulated by siRNA (Fig. 8A). Intriguingly,

Table 4
The differentially expressed proteins between the monoclonal L02 cells stably expressed the Flag-UCH37 fusion protein and the L02 cells carrying an empty vector.

Prot_acc	Prot_desc	Ratio (UCH37/Control)
IPI00935516	Tax_Id = 9606 Gene_Symbol = HSBP1 Heat shock factor-binding protein 1	1717.797
IPI00018963	Tax_Id = 9606 Gene_Symbol = PARVA Isoform 1 of Alpha-parvin	1717.797
IPI00060523	Tax_Id = 9606 Gene_Symbol = TLCD1 TLC domain-containing protein 1	3.081
IPI00299313	Tax_Id = 9606 Gene_Symbol = UCHL5 Isoform 1 of Ubiquitin carboxyl-terminal hydrolase isozyme L5	2.619
IPI00220528	Tax_Id = 9606 Gene_Symbol = SNRPF Small nuclear ribonucleoprotein F	2.489
IPI00025344	Tax_Id = 9606 Gene_Symbol = NDUFS6 NADH dehydrogenase [ubiquinone] iron–sulfur protein 6, mitochondrial	2.394
IPI00873472	Tax_Id = 9606 Gene_Symbol = SEC24A Isoform 1 of Protein transport protein Sec24A	2.236
IPI00004968	Tax_Id = 9606 Gene_Symbol = PRPF19 Pre-mRNA-processing factor 19	1.999
IPI00005793	Tax_Id = 9606 Gene_Symbol = AP3B2 AP-3 complex subunit beta-2	1.953
IPI00554723	Tax_Id = 9606 Gene_Symbol = SNORA70; RPL10 60S ribosomal protein L10	1.807
IPI00037283	Tax_Id = 9606 Gene_Symbol = DNM1L Isoform 5 of Dynamin-1-like protein	1.775
IPI00299468	Tax_Id = 9606 Gene_Symbol = SCD Acyl-CoA desaturase	1.738
IPI00470779	Tax_Id = 9606 Gene_Symbol = TXLNA Alpha-taxilin	1.678
IPI00030362	Tax_Id = 9606 Gene_Symbol = PLP2 Proteolipid protein 2	1.597
IPI00062599	Tax_Id = 9606 Gene_Symbol = −71 kDa protein	1.559
IPI00009922	Tax_Id = 9606 Gene_Symbol = C14orf156 SRA stem-loop-interacting RNA-binding protein, mitochondrial	1.526
IPI00304925	Tax_Id = 9606 Gene_Symbol = HSPA1B; HSPA1A Heat shock 70 kDa protein 1A/1B	1.517
IPI00015560	Tax_Id = 9606 Gene_Symbol = ELP2 Isoform 1 of Elongator complex protein 2	1.502
IPI00306127	Tax_Id = 9606 Gene_Symbol = THUMPD3 THUMP domain-containing protein 3	1.502
IPI00412713	Tax_Id = 9606 Gene_Symbol = SAMM50 Sorting and assembly machinery component 50 homolog	0.662
IPI00023344	Tax_Id = 9606 Gene_Symbol = SYMPK Isoform 1 of Symplekin	0.656
IPI00005715	Tax_Id = 9606 Gene_Symbol = UBE4B Isoform 1 of Ubiquitin conjugation factor E4 B	0.656
IPI00027681	Tax_Id = 9606 Gene_Symbol = NNMT Nicotinamide N-methyltransferase	0.653
IPI00384872	Tax_Id = 9606 Gene_Symbol = UGT1A7 UDP-glucuronosyltransferase 1-7	0.642
IPI00010863	Tax_Id = 9606 Gene_Symbol = ATOX1 Copper transport protein ATOX1	0.637
IPI00219673	Tax_Id = 9606 Gene_Symbol = GSTK1 Glutathione S-transferase kappa 1	0.63
IPI00006702	Tax_Id = 9606 Gene_Symbol = PELP1 cDNA FLJ56414, highly similar to Homo sapiens proline-, glutamic acid-, leucine-rich protein 1 (PELP1), mRNA	0.622
IPI00021347	Tax_Id = 9606 Gene_Symbol = UBE2L3 Ubiquitin-conjugating enzyme E2 L3	0.609
IPI00007423	Tax_Id = 9606 Gene_Symbol = ANP32B Isoform 1 of Acidic leucine-rich nuclear phosphoprotein 32 family member B	0.603
IPI00025815	Tax_Id = 9606 Gene_Symbol = TARDBP TDP43	0.6
IPI00154975	Tax_Id = 9606 Gene_Symbol = DNAJC9 DnaJ homolog subfamily C member 9	0.593
IPI00293350	Tax_Id = 9606 Gene_Symbol = TSNAX Translin-associated protein X	0.574
IPI00293276	Tax_Id = 9606 Gene_Symbol = MIF Macrophage migration inhibitory factor	0.563
IPI00218658	Tax_Id = 9606 Gene_Symbol = ITPR1 Isoform 2 of Inositol 1,4,5-trisphosphate receptor type 1	0.553
IPI00158615	Tax_Id = 9606 Gene_Symbol = THOC2 THO complex subunit 2	0.537
IPI00013160	Tax_Id = 9606 Gene_Symbol = LGTN Isoform 1 of Ligatin	0.513
IPI00064767	Tax_Id = 9606 Gene_Symbol = ARHGAP17 Isoform 1 of Rho GTPase-activating protein 17	0.492
IPI00019517	Tax_Id = 9606 Gene_Symbol = WT1 Isoform 1 of Wilms tumor protein	0.41
IPI00744711	Tax_Id = 9606 Gene_Symbol = PNPT1 Polyribonucleotide nucleotidyltransferase 1, mitochondrial	0.399
IPI00301489	Tax_Id = 9606 Gene_Symbol = UROD Uroporphyrinogen decarboxylase	0.002

Prot_acc, protein accession number; Prot_desc, protein description; UCH37, the monoclonal L02 cells stably expressed the Flag-UCH37 fusion protein; and control, the L02 cells carrying an empty vector.

the cell migratory and invasive abilities of L02-UCH37 cells transfected with PRP19 siRNA were significantly weakened (Fig. 8B–D). This finding was confirmed with two other independent PRP19 siRNA oligoribonucleotides (Supplementary Figs. 4, 5).

4. Discussion

Hepatocellular carcinoma (HCC) represents one of the most challenging cancers [25]. Ubiquitin C-terminal hydrolase 37 (UCH37) is a member of the ubiquitin C-terminal hydrolase (UCH) which is a subfamily of deubiquitinating enzymes (DUBs) [26–28]. Previous studies have shown its potential roles in oncogenesis. Rolén U et al. have found that the activity of the C-terminal hydrolases UCH37 is up-regulated in the majority of tumor tissues compared with the adjacent normal tissues [29]. Kapuria V et al. have found that WP1130, a partly selective DUB inhibitor which directly inhibits DUB activity of USP5, USP9x, USP14 and UCH37, could mediate inhibition of tumor-activated DUBs resulting in down-regulation of anti-apoptotic and up-regulation of proapoptotic proteins [30]. Chen Y and his colleagues have showed that the protein expression level of UCH37 was higher in the esophageal squamous cell carcinoma (ESCC) tissues than in para-tumorous tissues and that UCH37 was overexpressed in the tumor tissues of recurrence patients [31].

Here, we provided evidence for the first time that the HCC cancerous tissues had higher UCH37 expression relative to the adjacent para-cancerous tissues, which further confirmed the previous researches. The result of multivariate analysis also showed us that UCH37 could be a predictor for the time to recurrence (TTR) and had the potential power to predict the HCC recurrence after curative resection. Although some recognized factors, such as BCLC stage, TNM stage, encapsulation and vascular invasion were associated with overall survival (OS) and/or TTR in univariate analysis, they presented no statistical significance in multivariate analysis, most likely because of the limited number of patients enrolled in this study. Therefore, further investigation with a large-scale and longer follow-up study should be required to confirm its potential role in HCC recurrence.

As mentioned in the Introduction, previous work has showed that UCH37 possesses deubiquitinating activity via associating with the proteasome or hINO80. Some literature has also reported the biological roles and interactant of UCH37. The interaction between Smads and UCH37 could potentially counteract Smurf-mediated ubiquitination. UCH37 competes with Smurf2 in binding concurrently to Smad7 so that it deubiquitinates the activated type I TGF-β receptor, thereby rescuing it from proteasomal degradation. The up-regulation of TGF-β signaling by UCH37 could also be partly explained by the deubiquitination and stabilization of Smad3 [32,33]. UCH37 knockdown significantly

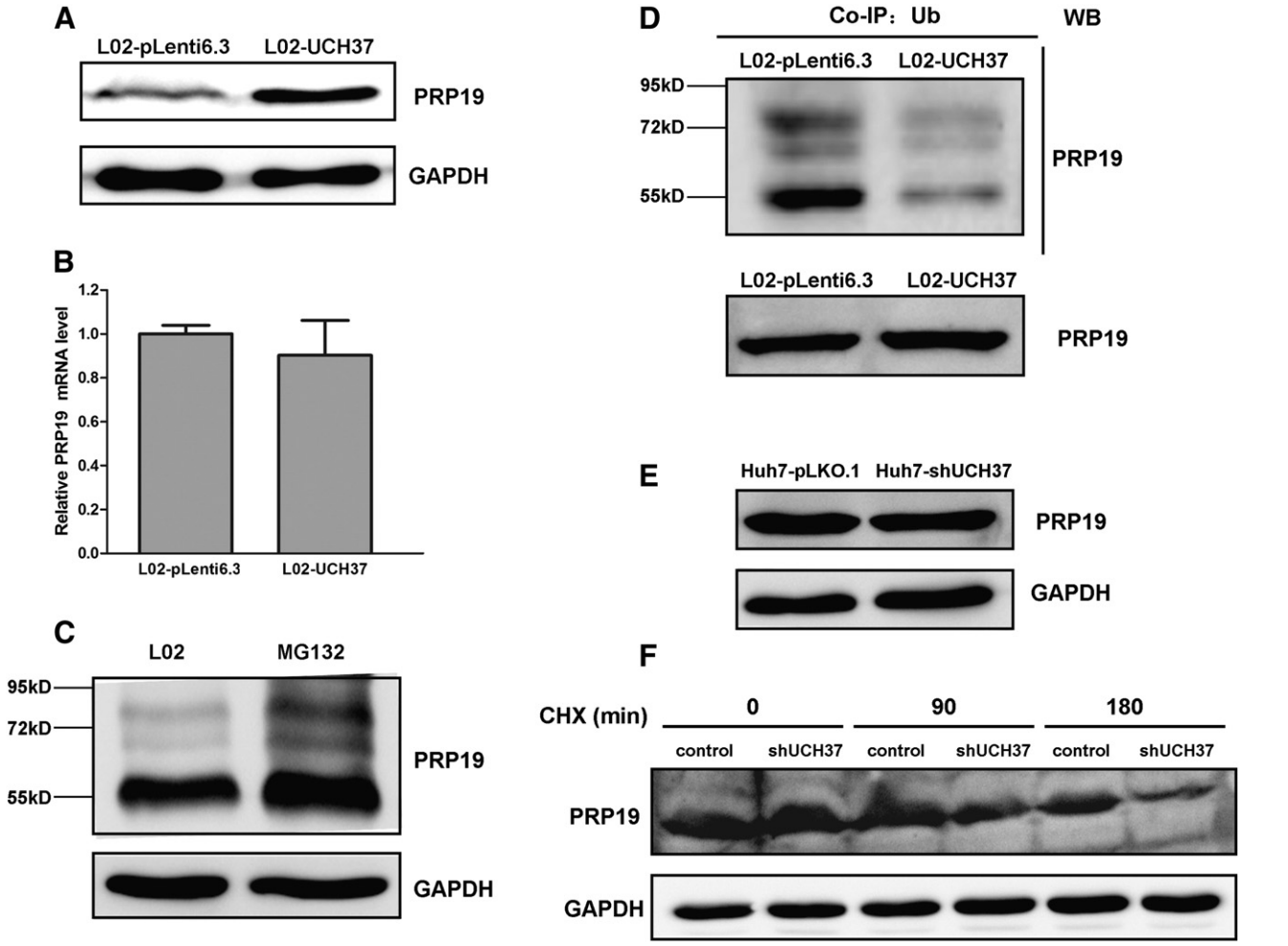

Fig. 6. UCH37 deubiquitinates PRP19. (A) Over-expression of UCH37 up-regulated PRP19. GAPDH was used as a loading control. (B) The mRNA level of PRP19 was assessed in the control cells and the treated L02 cells. Real-time PCR of β-actin mRNA expression was performed as a control. Data were presented as mean value ± SD. (C) The degradation of PRP19 was mediated through ubiquitin proteasome pathway. L02, L02 cells; MG132, L02 cells were treated in presence of MG132 (10 μmol/L) for 24 h. GAPDH was used as a loading control. (D) UCH37 deubiquitinated PRP19. For co-IP experiments using anti-Ub antibody, the level of PRP19 in the treated L02 cells was the same as that in the control cells. L02-pLenti6.3, L02 cells carrying an empty vector; L02-UCH37, the monoclonal L02 cells stably expressing Flag-UCH37 fusion protein. (E) The protein level of PRP19 was assessed in the control cells and Huh7-shUCH37 cells. GAPDH was used as a loading control. (F) PRP19 proteins from the control cells and Huh7-shUCH37 cells treated with 20 μM cycloheximide for different time intervals were analyzed by western blotting. Huh7-pLKO.1/control, Huh7 cells carrying an empty vector; Huh7-shUCH37/shUCH37, the stable monoclonal Huh7 cells whose UCH37 expression was down-regulated.

inhibits the activity of a TGF-β-dependent gene reporter and selectively decreases levels of some TGF-β-dependent target genes, notably p21, a protein which plays a key role in cell cycle arrest by preventing G1/S cell cycle progression and inhibits proliferation, and PAI-1, a scaffold protein that has been shown to act as a tumor suppressor and induce apoptosis via caspase-3, during the early phase of TGF-β receptor activation. Yet UCH37 knockdown significantly impairs cell migration in pancreatic cancer cell lines through the abolition of the TGF-β-induced expression of MMP-2 and PAI-1, which are thought to play a key role in TGF-β-dependent cell migration and tumor invasion, at both early and late stages of TGF-β receptor activation [34]. Chen Z et al. have showed that the ratio of Bax/Bcl-2 is higher in silencing of UCH37 than in that of control group after that of UCH37 in A549 cells. Meanwhile, experiments with the A549 cell line disclose that silencing of UCH37 could induce efficiently A549 cell apoptosis through activation of caspase-9 and caspase-3. On the other hand, over-expression of UCH37 leads to the opposite effect [35]. Recently, our group have showed that the quantity of UCH37 rises in HCC using a functional proteomic analysis to screen UCH37-interacting proteins in HCC, thus identifying glucose-regulated protein 78 (GRP78), essential for cell viability, as one interacting with UCH37 [36]. All of the evidences suggest that the up-regulation of UCH37 may play an important role in oncogenesis through promoting some proto-oncogenes' expression and stem cell-like characteristics in the cell.

In our study, UCH37 was found to promote cell migration and invasion in HCC cells in vitro, which was consistent with the results of immunohistochemistry in our clinical research. To better understand the effect of UCH37 on quantitative protein changes in HCC, we utilized the differential proteomics which is Isobaric Tag for Relative and Absolute Quantitation (iTRAQ) in combination with LC–MS/MS. iTRAQ has gained popularity for its ability to perform concurrent identification and relative quantification of hundreds of proteins [37–40], and has been employed in several oncoproteomics studies [41–44]. iTRAQ data showed that the differentially expressed proteins (19 up-regulated and 21 down-regulated) were widely distributed in the cell, and demonstrated that they played a role in all aspects of cell biology, indicating that UCH37 were involved in almost all biological processes.

As mentioned above, PRP19 was chosen for further study. PRP19, a core component of the spliceosomal NineTeen associated-Complex (NTC) [45,46], plays a direct role in the activation and structural stabilization of the spliceosome [47–50]. Previous studies have indicated that PRP19 complex is associated with tumorigenesis. It is a tempting hypothesis that aberrant splicing results in inaccurate sister chromatid segregation, thereby leading to tumorigenesis [51,52]. On the

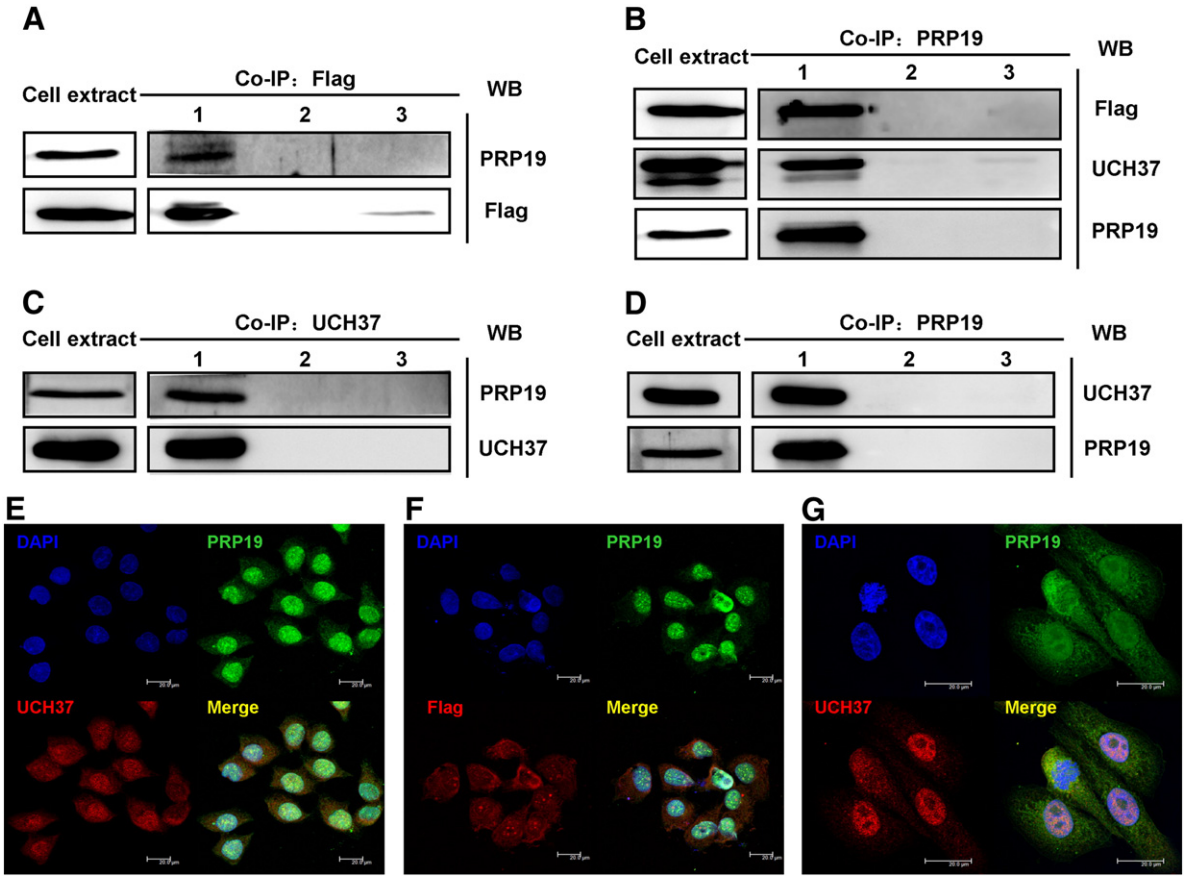

Fig. 7. UCH37 interacts with PRP19. (A) The cell lysates from L02-UCH37 cells were co-immunoprecipitated with anti-Flag antibody and immunoblotted with anti-Flag and anti-PRP19 antibodies, respectively. Lane 1, Flag-immunoprecipitates from L02-UCH37 cells; lane 2, the cell lysates from L02-UCH37 cells co-immunoprecipitated with isotype control antibody; lane 3, the cell lysates from L02-UCH37 cells co-immunoprecipitated with PBS. (B) The cell lysates from L02-UCH37 cells were co-immunoprecipitated with anti-PRP19 antibody and immunoblotted with anti-PRP19, anti-Flag and anti-UCH37 antibodies, respectively. Lane 1, PRP19-immunoprecipitates from L02-UCH37 cells; lane 2, the cell lysates from L02-UCH37 cells co-immunoprecipitated with isotype control antibody; lane 3, the cell lysates from L02-UCH37 cells co-immunoprecipitated with PBS. (C and D) The interaction of UCH37 with PRP19 with endogenously UCH37 was confirmed in Huh7 cells via co-immunoprecipitation. (E and F) Co-localization of Flag-UCH37 fusion protein and PRP19 was examined by confocal laser scanning microscopy analysis in L02-UCH37 cells. (G) Co-localization of UCH37 with PRP19 with endogenously UCH37 was examined by confocal laser scanning microscopy analysis in Huh7 cells. A merged image was illustrated by yellow signal and nuclei were visualized by DAPI. The magnification was 945 (E and F) and 1890 (G), and the length of the scale bar was 20 μm.

other hand, PRP19 complex has an essential function in the processing of DNA lesions particularly DNA interstrand cross-links (ICLs) [53–55]. It has been previously reported that over-expression of PRP19 complex increases cellular lifespan in human cells possibly by enhancing DNA repair capacity [56]. Otherwise, PRP19 complex has been recently found to be involved in DNA damage checkpoint signaling pathways [57]. Thus, PRP19 complex functions in two aspects of the DNA damage response (DDR), namely DNA repair and checkpoint signaling.

In the current study, we observed that the deubiquitination of PRP19 was regulated by UCH37. Furthermore, PRP19 was identified as one of UCH37-interacting proteins, which was confirmed by co-IP and confocal laser scanning microscopy analysis (both over-expressed and endogenous). To determine the relationship between UCH37, PRP19 and the capability of cell migration and invasion, the expression of PRP19 in L02-UCH37 cells was down-regulated by siRNA. Intriguingly, knock-down of PRP19 reduced the capability of cell migration and invasion, compare with the control cells, suggesting that UCH37 exerted its effects at least in part by deubiquitinating and stabilizing PRP19.

Taken together, the results of this study demonstrated that UCH37 could promote cell migration and invasion in HCC cell lines through interacting and deubiquitinating PRP19. Furthermore, it is in HCC that we first reported UCH37 could be a predictive marker of HCC recurrence after curative resection. We believe that UCH37 could be a good diagnostic and therapeutic target for controlling HCC recurrence, and further investigations in this field are needed.

5. Conclusion

This study provided evidence for the first time that UCH37 could promote cell migration and invasion in HCC cell lines through interacting and deubiquitinating PRP19, and this is the first report showing UCH37 as a predictive marker of HCC recurrence in HCC patients after curative resection.

Supplementary data to this article can be found online at http://dx.doi.org/10.1016/j.bbamcr.2012.11.020.

Disclosures

The authors have no financial conflicts of interest. The current study was approved by the Institutional Ethics Committee of Zhongshan Hospital, Fudan University.

Acknowledgements

The authors would like to thank the members of Prof. Xizhong Shen's laboratory for their helpful discussion and critical reading of the manuscript, and the members of the Key Laboratory of Molecular

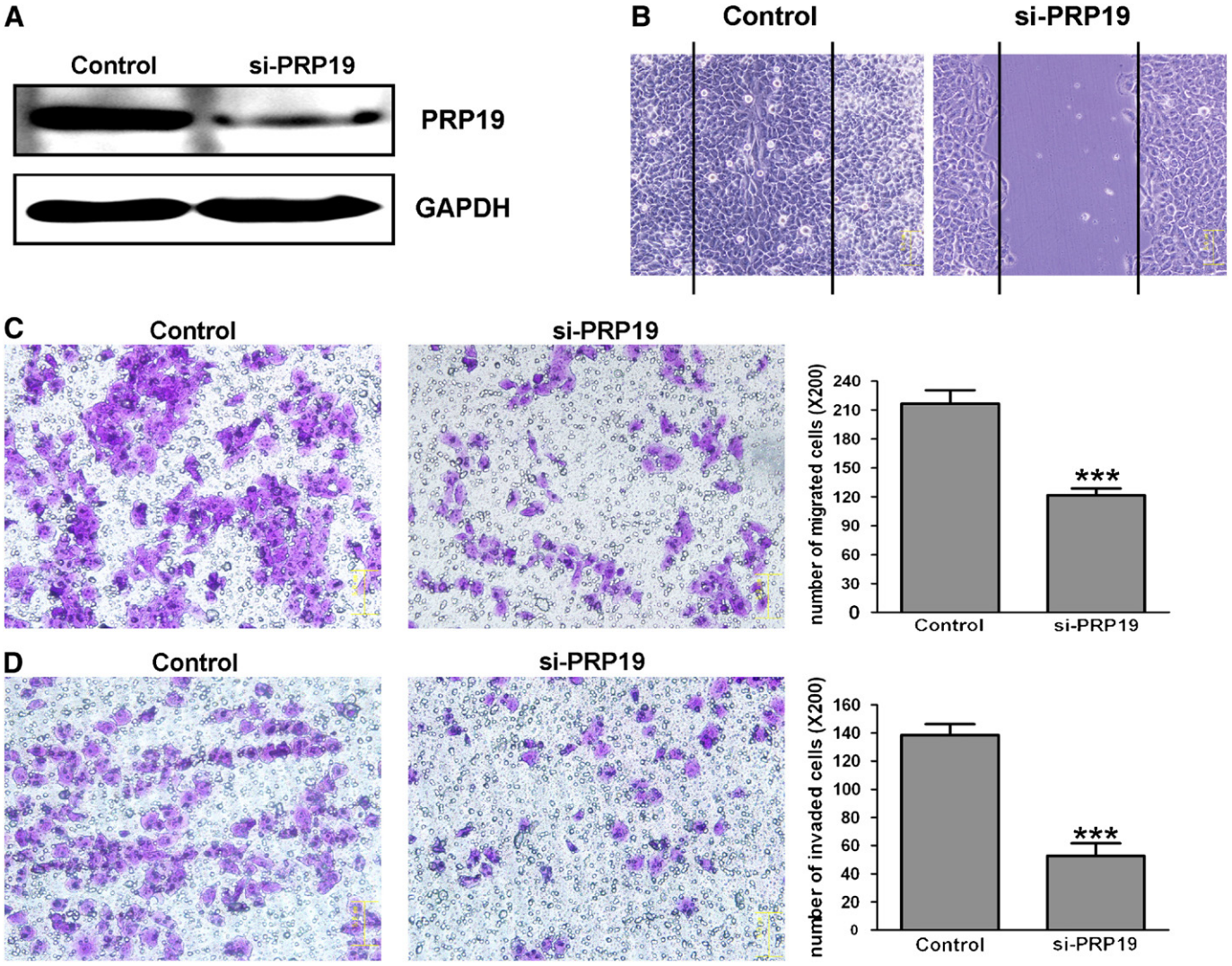

Fig. 8. PRP19 is involved in UCH37-induced HCC cell migration and invasion. (A) L02-UCH37 cells were transfected with PRP19 siRNA-1 or control siRNA for 48 h. GAPDH was used as a loading control. (B) Confluent L02-UCH37 monolayers transfected with PRP19 siRNA or control siRNA were scratch wounded at 48 h after transfection. Photographs were taken at 48 h after wounding. (C and D) L02-UCH37 cells transfected with PRP19 siRNA or control siRNA were seeded in the top chamber with a non-coated membrane or a Matrigel-coated membrane and allowed to migrate or invade for 48 h. Migrated or invaded cells were stained by crystal violet (left and middle, representative images of three independent experiments were shown). The magnification was 200. The number of migrated or invaded cells was manually counted in four independent fields per well with light microscope (right). Columns represented the average of four random fields; bars, SD; Control, L02-UCH37 cells transfected with control siRNA; si-PRP19, L02-UCH37 cells transfected with PRP19 siRNA. *** $p<0.001$.

Medicine (under the auspice of the Ministry of Education), Shanghai Medical School of Fudan University for their technical assistance and Institutes of Biomedical Sciences, Fudan University for their confocal laser scanning microscopy. The study was partly funded by Shanghai Science and Technology Commission (10410709400; 10411950100), National Nature Science Foundation of China (no. 81000968; no. 81101540; no. 81101637; no. 81172273; no. 81272388) and the National Clinical Key Special Subject of China.

References

[1] J.M. Llovet, A. Burroughs, J. Bruix, Hepatocellular carcinoma, Lancet 362 (2003) 1907–1917.
[2] H.B. El-Serag, Hepatocellular carcinoma: recent trends in the United States, Gastroenterology 127 (2004) S27–S34.
[3] Z.Y. Tang, S.L. Ye, Y.K. Liu, L.X. Qin, H.C. Sun, Q.H. Ye, L. Wang, J. Zhou, S.J. Qiu, Y. Li, X.N. Ji, H. Liu, J.L. Xia, Z.Q. Wu, J. Fan, Z.C. Ma, X.D. Zhou, Z.Y. Lin, K.D. Liu, A decade's studies on metastasis of hepatocellular carcinoma, J. Cancer Res. Clin. Oncol. 130 (2004) 187–196.
[4] Y. Yang, H. Nagano, H. Ota, O. Morimoto, M. Nakamura, H. Wada, T. Noda, B. Damdinsuren, S. Marubashi, A. Miyamoto, Y. Takeda, K. Dono, K. Umeshita, S. Nakamori, K. Wakasa, M. Sakon, M. Monden, Patterns and clinicopathologic features of extrahepatic recurrence of hepatocellular carcinoma after curative resection, Surgery 141 (2007) 196–202.
[5] Q.H. Ye, L.X. Qin, M. Forgues, P. He, J.W. Kim, A.C. Peng, R. Simon, Y. Li, A.I. Robles, Y. Chen, Y. Chen, Z.C. Ma, Z.Q. Wu, S.L. Ye, Y.K. Liu, Z.Y. Tang, X.W. Wang, Predicting hepatitis B virus-positive metastatic hepatocellular carcinomas using gene expression profiling and supervised machine learning, Nat. Med. 9 (2003) 416–423.
[6] Q. Gao, S.J. Qiu, J. Fan, J. Zhou, X.Y. Wang, Y.S. Xiao, Y. Xu, Y.W. Li, Z.Y. Tang, Intratumoral balance of regulatory and cytotoxic T cells is associated with prognosis of hepatocellular carcinoma after resection, J. Clin. Oncol. 25 (2007) 2586–2593.
[7] X.R. Yang, Y. Xu, G.M. Shi, J. Fan, J. Zhou, Y. Ji, H.C. Sun, S.J. Qiu, B. Yu, Q. Gao, Y.Z. He, W.Z. Qin, R.X. Chen, G.H. Yang, B. Wu, Q. Lu, Z.Q. Wu, Z.Y. Tang, Cytokeratin 10 and cytokeratin 19: predictive markers for poor prognosis in hepatocellular carcinoma patients after curative resection, Clin. Cancer Res. 14 (2008) 3850–3859.
[8] S.Y. Peng, W.J. Chen, P.L. Lai, Y.M. Jeng, J.C. Sheu, H.C. Hsu, High a-fetoprotein level correlates with high stage, early recurrence and poor prognosis of hepatocellular carcinoma: significance of hepatitis virus infection, age, p53, and β-catenin mutations, Int. J. Cancer 112 (2004) 44–50.
[9] L.X. Qin, Z.Y. Tang, Recent progress in predictive biomarkers for metastatic recurrence of human hepatocellular carcinoma: a review of the literature, J. Cancer Res. Clin. Oncol. 130 (2004) 497–513.
[10] A. Hershko, A. Ciechanover, The ubiquitin system, Annu. Rev. Biochem. 67 (1998) 425–479.
[11] C.M. Pickart, Mechanisms underlying ubiquitination, Annu. Rev. Biochem. 70 (2001) 503–533.

[12] D. Finley, A. Ciechanover, A. Varshavsky, Ubiquitin as a central cellular regulator, Cell 116 (2004) S29–S32, (2–32).
[13] V.V. Sridhar, A. Kapoor, K. Zhang, J. Zhu, T. Zhou, P.M. Hasegawa, R.A. Bressan, J.K. Zhu, Control of DNA methylation and heterochromatic silencing by histone H2B deubiquitination, Nature 447 (2007) 735–738.
[14] H. Liu, R. Buus, M.J. Clague, S. Urbe, Regulation of ErbB2 receptor status by the proteasomal DUB POH1, PLoS One 4 (2009) e5544.
[15] S. Singhal, M.C. Taylor, R.T. Baker, Deubiquitylating enzymes and disease, BMC Biochem. 9 (Suppl. 1) (2008) S3.
[16] C.N. Larsen, B.A. Krantz, K.D. Wilkinson, Substrate specificity of deubiquitinating enzymes: ubiquitin C-terminal hydrolases, Biochemistry-Us 37 (1998) 3358–3368.
[17] T. Yao, L. Song, W. Xu, G.N. DeMartino, L. Florens, S.K. Swanson, M.P. Washburn, R.C. Conaway, J.W. Conaway, R.E. Cohen, Proteasome recruitment and activation of the Uch37 deubiquitinating enzyme by Adrm1, Nat. Cell Biol. 8 (2006) 994–1002.
[18] P. Schreiner, X. Chen, K. Husnjak, L. Randles, N. Zhang, S. Elsasser, D. Finley, I. Dikic, K.J. Walters, M. Groll, Ubiquitin docking at the proteasome through a novel pleckstrin-homology domain interaction, Nature 453 (2008) 548–552.
[19] K. Husnjak, S. Elsasser, N. Zhang, X. Chen, L. Randles, Y. Shi, K. Hofmann, K.J. Walters, D. Finley, I. Dikic, Proteasome subunit Rpn13 is a novel ubiquitin receptor, Nature 453 (2008) 481–488.
[20] T. Yao, L. Song, J. Jin, Y. Cai, H. Takahashi, S.K. Swanson, M.P. Washburn, L. Florens, R.C. Conaway, R.E. Cohen, J.W. Conaway, Distinct modes of regulation of the Uch37 deubiquitinating enzyme in the proteasome and in the Ino80 chromatin-remodeling complex, Mol. Cell 31 (2008) 909–917.
[21] V.P. Zediak, S.L. Berger, Hit and run: transient deubiquitylase activity in a chromatin-remodeling complex, Mol. Cell 31 (2008) 773–774.
[22] Y. Fang, D. Fu, X.Z. Shen, The potential role of ubiquitin c-terminal hydrolases in oncogenesis, Biochim. Biophys. Acta 1806 (2010) 1–6.
[23] M. Ashburner, C.A. Ball, J.A. Blake, D. Botstein, H. Butler, J.M. Cherry, A.P. Davis, K. Dolinski, S.S. Dwight, J.T. Eppig, M.A. Harris, D.P. Hill, L. Issel-Tarver, A. Kasarskis, S. Lewis, J.C. Matese, J.E. Richardson, M. Ringwald, G.M. Rubin, G. Sherlock, Gene ontology: tool for the unification of biology. The Gene Ontology Consortium, Nat. Genet. 25 (2000) 25–29.
[24] M. Kanehisa, S. Goto, S. Kawashima, Y. Okuno, M. Hattori, The KEGG resource for deciphering the genome, Nucleic Acids Res. 32 (2004) D277–D280.
[25] A. Jemal, R. Siegel, E. Ward, T. Murray, J. Xu, M.J. Thun, Cancer statistics, 2007, CA, Cancer J. Clin. 57 (2007) 43–66.
[26] A.Y. Amerik, M. Hochstrasser, Mechanism and function of deubiquitinating enzymes, Biochim. Biophys. Acta 1695 (2004) 189–207.
[27] T.A. Soboleva, R.T. Baker, Deubiquitinating enzymes: their functions and substrate specificity, Curr. Protein Pept. Sci. 5 (2004) 191–200.
[28] S.M. Nijman, M.P. Luna-Vargas, A. Velds, T.R. Brummelkamp, A.M. Dirac, T.K. Sixma, R. Bernards, A genomic and functional inventory of deubiquitinating enzymes, Cell 123 (2005) 773–786.
[29] U. Rolen, V. Kobzeva, N. Gasparjan, H. Ovaa, G. Winberg, F. Kisseljov, M.G. Masucci, Activity profiling of deubiquitinating enzymes in cervical carcinoma biopsies and cell lines, Mol. Carcinog. 45 (2006) 260–269.
[30] V. Kapuria, L.F. Peterson, D. Fang, W.G. Bornmann, M. Talpaz, N.J. Donato, Deubiquitinase inhibition by small-molecule WP1130 triggers aggresome formation and tumor cell apoptosis, Cancer Res. 70 (2010) 9265–9276.
[31] Y. Chen, D. Fu, J. Xi, Z. Ji, T. Liu, Y. Ma, Y. Zhao, L. Dong, Q. Wang, X. Shen, Expression and clinical significance of UCH37 in human esophageal squamous cell carcinoma, Dig. Dis. Sci. 57 (2012) 2310–2317.
[32] S.J. Wicks, K. Haros, M. Maillard, L. Song, R.E. Cohen, P.T. Dijke, A. Chantry, The deubiquitinating enzyme UCH37 interacts with Smads and regulates TGF-beta signaling, Oncogene 24 (2005) 8080–8084.
[33] S.J. Wicks, T. Grocott, K. Haros, M. Maillard, D.P. Ten, A. Chantry, Reversible ubiquitination regulates the Smad/TGF-beta signalling pathway, Biochem. Soc. Trans. 34 (2006) 761–763.
[34] A.J. Cutts, S.M. Soond, S. Powell, A. Chantry, Early phase TGFβ receptor signalling dynamics stabilised by the deubiquitinase UCH37 promotes cell migratory responses, Int. Biochem. Cell Biol. 43 (2011) 604–612.
[35] Z. Chen, X. Niu, Z. Li, Y. Yu, X. Ye, S. Lu, Z. Chen, Effect of ubiquitin carboxy-terminal hydrolase 37 on apoptotic in A549 cells, Cell Biochem. Funct. 29 (2011) 142–148.
[36] Y. Fang, J. Mu, Y. Ma, D. Ma, D. Fu, X. Shen, The interaction between ubiquitin C-terminal hydrolase 37 and glucose-regulated protein 78 in hepatocellular carcinoma, Mol. Cell. Biochem. 359 (2012) 59–66.
[37] A.M. Boehm, S. Putz, D. Altenhofer, A. Sickmann, M. Falk, Precise protein quantification based on peptide quantification using iTRAQ, BMC Bioinformatics 8 (2007) 214.
[38] C.S. Gan, P.K. Chong, T.K. Pham, P.C. Wright, Technical, experimental, and biological variations in isobaric tags for relative and absolute quantitation (iTRAQ), J. Proteome Res. 6 (2007) 821–827.
[39] S. Wiese, K.A. Reidegeld, H.E. Meyer, B. Warscheid, Protein labeling by iTRAQ: a new tool for quantitative mass spectrometry in proteome research, Proteomics 7 (2007) 340–350.
[40] C.L. Han, C.W. Chien, W.C. Chen, Y.R. Chen, C.P. Wu, H. Li, Y.J. Chen, A multiplexed quantitative strategy for membrane proteomics: opportunities for mining therapeutic targets for autosomal dominant polycystic kidney disease, Mol. Cell. Proteomics 7 (2008) 1983–1997.
[41] R. Ralhan, L.V. Desouza, A. Matta, T.S. Chandra, S. Ghanny, G.S. Datta, S. Bahadur, K.W. Siu, Discovery and verification of head-and-neck cancer biomarkers by differential protein expression analysis using iTRAQ labeling, multidimensional liquid chromatography, and tandem mass spectrometry, Mol. Cell. Proteomics 7 (2008) 1162–1173.
[42] C.W. Sutton, N. Rustogi, C. Gurkan, A. Scally, M.A. Loizidou, A. Hadjisavvas, K. Kyriacou, Quantitative proteomic profiling of matched normal and tumor breast tissues, J. Proteome Res. 9 (2010) 3891–3902.
[43] W.W. Goh, Y.H. Lee, R.M. Zubaidah, J. Jin, D. Dong, Q. Lin, M.C. Chung, L. Wong, Network-based pipeline for analyzing MS data: an application toward liver cancer, J. Proteome Res. 10 (2011) 2261–2272.
[44] K.H. Chiu, Y.H. Chang, Y.S. Wu, S.H. Lee, P.C. Liao, Quantitative secretome analysis reveals that COL6A1 is a metastasis-associated protein using stacking gel-aided purification combined with iTRAQ labeling, J. Proteome Res. 10 (2011) 1110–1125.
[45] S.P. Chan, D.I. Kao, W.Y. Tsai, S.C. Cheng, The Prp19p-associated complex in spliceosome activation, Science 302 (2003) 279–282.
[46] O.V. Makarova, E.M. Makarov, H. Urlaub, C.L. Will, M. Gentzel, M. Wilm, R. Luhrmann, A subset of human 35S U5 proteins, including Prp19, function prior to catalytic step 1 of splicing, EMBO J. 23 (2004) 2381–2391.
[47] S.P. Chan, S.C. Cheng, The Prp19-associated complex is required for specifying interactions of U5 and U6 with pre-mRNA during spliceosome activation, J. Biol. Chem. 280 (2005) 31190–31199.
[48] S. Valadkhan, Y. Jaladat, The spliceosomal proteome: at the heart of the largest cellular ribonucleoprotein machine, Proteomics 10 (2010) 4128–4141.
[49] S. Chanarat, M. Seizl, K. Straber, The Prp19 complex is a novel transcription elongation factor required for TREX occupancy at transcribed genes, Genes Dev. 25 (2011) 1147–1158.
[50] C.J. David, A.R. Boyne, S.R. Millhouse, J.L. Manley, The RNA polymerase II C-terminal domain promotes splicing activation through recruitment of a U2AF65–Prp19 complex, Genes Dev. 25 (2011) 972–983.
[51] T.A. Cooper, L. Wan, G. Dreyfuss, RNA and disease, Cell 136 (2009) 777–793.
[52] S. Confalonieri, M. Quarto, G. Goisis, P. Nuciforo, M. Donzelli, G. Jodice, G. Pelosi, G. Viale, S. Pece, P.P. Di Fiore, Alterations of ubiquitin ligases in human cancer and their association with the natural history of the tumor, Oncogene 28 (2009) 2959–2968.
[53] X. Lu, R.J. Legerski, The Prp19/Pso4 core complex undergoes ubiquitylation and structural alterations in response to DNA damage, Biochem. Biophys. Res. Commun. 354 (2007) 968–974.
[54] N. Zhang, R. Kaur, X. Lu, X. Shen, L. Li, R.J. Legerski, The Pso4 mRNA splicing and DNA repair complex interacts with WRN for processing of DNA interstrand cross-links, J. Biol. Chem. 280 (2005) 40559–40567.
[55] K.N. Mahajan, B.S. Mitchell, Role of human Pso4 in mammalian DNA repair and association with terminal deoxynucleotidyl transferase, Proc. Natl. Acad. Sci. U. S. A. 100 (2003) 10746–10751.
[56] R. Voglauer, M.W. Chang, B. Dampier, M. Wieser, K. Baumann, T. Sterovsky, M. Schreiber, H. Katinger, J. Grillari, SNEV overexpression extends the life span of human endothelial cells, Exp. Cell Res. 312 (2006) 746–759.
[57] R.J. Legerski, The Pso4 complex splices into the DNA damage response, Cell Cycle 8 (2009) 3448–3449.